Separation and Purification Technology 284 (2022) 120273

Contents lists available at ScienceDirect

Separation and Purification Technology

journal homepage: www.elsevier.com/locate/seppur

Clarification of yeast cell suspensions by a highly porous polyamide nanofiber sponge

S. Mousavi [a], L. Filipová [a], J. Ebert [a], F.J. Heiligtag [b], R. Daumke [b], W. Loser [b], B. Ledergerber [b], B. Frank [b], C. Adlhart [a,*]

[a] Institute of Chemistry and Biotechnology, Zurich University of Applied Sciences ZHAW, 8820 Wädenswil, Switzerland
[b] Filtrox AG, Moosmühlestrasse 6, 9001 St. Gallen, Switzerland

ARTICLE INFO

Keywords:
Yeast cell filtration
Nanofibrous polyamide sponge
Depth filtration
Pore blocking mechanism
3D nanofiber aerogel

ABSTRACT

Depth filtration is an attractive method for initial clarification of broth for removing cells and cell debris. Electrospun nanofibers with their large specific surface area and a porous structure are known as attractive materials in filtration processes. However, dead-end filtration of cells through nanofiber mats (NFM) always leads to cake formation and increasing resistance. In this study, for the first time, a nanofiber sponge (NFS) or nanofiber aerogel was synthetized from polyamide 6 (PA6) building blocks. The NFS was flexible, highly porous and mechanically stable. The pore size of the NFS was tuned between 8 and 26 μm during the cryogenic processing step. Volumetric flux and filtration efficiency of the NFS depended on the pore size and the results were compared with those for NFM from the same PA6 nanofiber material. Dead-end filtration of *Saccharomyces cerevisiae* was feasible at a low differential pressure of 3.5 kPa and cell filtration efficiency was > 99 %. Modelling of the filtration process revealed that cake formation is prevented by NFS filters since cells are able to penetrate into the filter and to adsorb on their internal surface. The filtration characteristics were also compared with commercial depth filters and revealed the high flux of NFS filters along with the possibility to avoid filter aids and a low environmental impact. PA6-NFS filters may become a new and cost effective generation of filters for removing different cells or cell debris from broth and other applications.

1. Introduction

Separation of cells from fermenter suspensions is crucial in fermentation industry. Several methods such as centrifugation and filtration are used for the clarification of cell cultures. Regarding the high capital costs and operational limitations of centrifugation, filtration is known as one of the best industrial methods for removing yeast cells [1,2]. For this purpose, different types of organic and inorganic membranes have been studied. Bello and coworkers used polyimide hollow membranes for yeast filtration and found them more effective than centrifugation [3]. Sanjeev *et al.* [4] reported high yeast removal capacities for polypropylene membranes. Inorganic materials such as ceramics, alumina, zirconia, and glass membranes have been also used for yeast cell filtration [5]. Despite high retention capacities reported for some membranes, rapid surface fouling has limited their industrial application [6,7]. In order to reduce the tendency of cells for making impermeable cakes, different solutions have been proposed. Filter aids are known as a common industrial solution, which work as a pre-coat to protect filters from blocking [8]. However, the costs of filter aids, additional process elaboration, and the need for removing them adds extra difficulties to the process. Improvement was achieved with mixed beds. For instance, Mota *et al.* used a mixed bed with glass balls to increase removal efficiency [9]. Alternatively, several studies report the fabrication of specifically patterned membranes with well-defined pore geometry and spacing to increase flux and removal efficiency of filters [10–12]. Although pore geometry did influence the pore blockage regime of the initial filtration processes, the follow up cake formation remained problematic.

Besides having appropriate structures, the choice of filter material plays an important role in filtration processes. Polyamide 6 (PA6) is an important thermoplastic with excellent solvent resistance and good processability. However, until now, it has only occasionally been used as cell filtration membrane. Due to the swallowing tendency of PA6 fibers in contact with water and the consequent blockage of the membrane

* Corresponding author.
E-mail address: christian.adlhart@zhaw.ch (C. Adlhart).

https://doi.org/10.1016/j.seppur.2021.120273
Received 20 September 2021; Received in revised form 2 December 2021; Accepted 6 December 2021
Available online 7 December 2021
1383-5866/© 2021 The Author(s). Published by Elsevier B.V. This is an open access article under the CC BY license (http://creativecommons.org/licenses/by/4.0/).

pores, industrial applications are restricted [13]. Nevertheless, Lemma and his group [14] reported separation of yeast cells from beer samples through dead-end filtration using electrospun PA6 nanofibers. They claimed efficient initial yeast cell filtration, but increasing resistance due to the formation of a cake layer was not avoidable.

In order to increase mass transport and overcome the problems associated with pore blocking and cake formation, nanofiber sponges (NFS, also termed nanofiber aerogels) might be an interesting alternative. NFS are the 3D counterparts of the essentially flat nanofiber mats (NFM, also termed membranes). They are made from the same nanofiber building blocks, but their structure is highly porous, often containing larger cellular pores. They have been made from several polymer materials, e.g. polyacrylonitrile/SiO_2 [15], poly(MA-*co*-MMA-*co*-MABP) [16], pullulan/PVA [17], PCL/gelatin [18], chitosan [19]. A recent summary on NFS materials is given by Dilamian *et al.* [20]. A number of filtration or separation applications have been reported for NFS, such as aerosol filtration [17,21], oil/water separation [15,22–25], dye adsorption [26], or microplastics [19]. In general, high separation efficiency and high flux were achieved. However, none of those studies has ever investigated the behavior of NFS for the filtration of particle matter in fluids such as yeast cells from a broth. And regarding the material aspect, NFS from PA6 have never been reported in the scientific literature, despite the wide application of PA6.

In the current study, we report the synthesis and characterization of PA6 NFS with tuned pore size. The highly flexible and porous NFS were evaluated for the dead-end filtration of yeast cell suspension and compared with electrospun NFM. High flux was achieved at a low hydrostatic pressure of 3.5 kPa. The decline of flux with filtration time was modelled with different blocking models such as cake filtration, complete blocking, intermediate blocking, and standard blocking showing that cake formation was successfully prevented with the PA6 NFS filters.

2. Materials and methods

2.1. Materials

PA6 (Ultramid B24 N 03) was obtained from Elmarco Ltd., Czech Republic. Dioxane, acetic acid, formic acid, sodium hydroxide (NaOH), and hydrochloric acid, (HCl, ACS reagent 37 %) were obtained from Merck, Switzerland. Normal active dry baker's yeast, *Saccharomyces cerevisiae*, was obtained from Lallemand Inc., Canada. Commercial depths filtration sheets, filtration capsules, and filter aids (see Table 2) were obtained from Eaton (Langenlonsheim, Germany), Pall Corporation (Port Washington, USA), and Filtrox AG (St. Gallen).

2.2. Yeast cell suspensions

Yeast cell suspensions with a mass concentration of $\gamma \approx 1.5$ g l^{-1} dry cell content were prepared by suspending the yeast cells in deionized water (pH = 5.7). The suspension was shacked with an orbital shaker for 10 min at 200 rpm.

2.3. Nanofiber sponge preparation

Producing three-dimensional structures from electrospun nanofibers through a freeze casting method was recently reported for different polymers [17,21,26]. In this work, PA6 nanofibers mats (NFM) were produced using free surface electrospinning (Fig. 1; for spinning conditions see Supporting Information). NFM were cut into small pieces and further chopped and homogenized in a mixture of water/dioxane (20 wt % dioxane) using a high speed homogenizer (IKA T25, S25N-25F, IKA GmbH, Germany). Suspensions with a nominal fiber mass concentration of $\gamma = 10$ g l^{-1} were then cast into aluminum molds ($d = 50$ mm) and unidirectionally frozen from the bottom. Water/dioxane crystals were removed through freeze-drying leaving cellular pores with walls of cut PA6 nanofibers. To achieve a mechanically stable NFS, the NFS green body was cross-linked at 210 °C for 45 min.

2.4. Yeast cell filtration

Filtration of yeast cell suspensions was performed at room temperature with a hydrostatic pressure of 3.5 kPa (see Supporting Information). Flowrate and filtration efficiency were determined each 10 or 40 ml by time interval and turbidity, measured with a turbidimeter TN-100 (Eutech Instruments, Netherlands). For commercial depth filters, the filtration efficiency was determined at the endpoint at a throughput of 140 l m^{-2}. In case of alluvial filtration, Celpure® had been added at a mass ratio 4:1 with respect to yeast dry mass.

2.5. Characterization

Morphology of NFM and NFS was assessed by scanning electron microscopy (SEM) using a FEI Quanta FEG 250 (Thermo Fisher Scientific, USA); samples were sputter coated with gold, accelerating voltage for image recording was 5 kV. Pore size was determined from SEM images using the software ImageJ by measuring 400 different pores from 5 different images. Among different techniques (e.g. mercury intrusion porosimetry, or micro-CT), SEM images have been frequently used and reported as a promising method with some potential advantages over the other available approaches [27,28].

NFM thickness was determined from cross sections by optical microscopy (20 measurements): a piece of NFM was cut in approx. 1 cm × 1 cm pieces, dipped into cryo gel and fast frozen with liquid nitrogen. The frozen samples were sectioned in a cryostat microtome (Microm HM550, Thermo Fischer Scientific, USA) into pieces with 10 μm thickness at −18 °C and mounted on the microscope slides (Supporting Information, Figure S1).

The electrokinetic surface potential (zeta-potential or ζ-potential) was determined as streaming potential. For NFS, a Mütek^{TM} SZP-06 (BTG-Voith, Germany) instrument was used while yeast cell suspensions were analyzed with a Zetasizer Nano ZS (Malvern Instruments, UK). The pH was adjusted using HCl and NaOH.

Differential scanning calorimetry (DSC, Mettler Toledo, Switzerland) characterization was done under nitrogen with a flow rate of 50 ml min^{-1} while the furnace temperature was increased from room temperature to 400 °C (heating rate of 10 °C min^{-1}).

Compression tests were performed with a TA.XTplus texture analyzer from Stable Micro Systems Ltd., UK. The Texture analyzer was calibrated at 500 N and equipped with a cylindrical probe with a diameter of 50 mm. The compression speed was set at 2 mm s^{-1} with

Table 1
Physical parameters of PA6 nanofiber based filter materials.

Filter type	Filter name	Bulk density ρ_b / mg cm^{-3}	Freezing temperature / °C	Pore diameter d / μm	Specific surfaces area a_{BET} / m^2 g^{-1}	BET constant C	Thickness l	Relative water value J_∞/J_0
nanofiber sponge	NFS-26	16.6 ± 1.3	−40	26 ± 14	13	12	2.0 ± 0.2 cm	1.00 ± 0.24
	NFS-8	17.3 ± 0.8	−110	8.3 ± 7.3	15	18	2.0 ± 0.2 cm	1.00 ± 0.28
nanofiber mat	NFM-5	275 ± 20	n.a.	5.3 ± 2.9	13	12	44 ± 7 μm	0.85 ± 0.24

Table 2
Saccharomyces cerevisiae dead-end filtration performance and *E*-factor of NFS, NFM and commercial depths filters at 3.5 kPa determined at a throughput of 140 l m^{-2}.

Filter type	Name	Supplier	Filtration application	*E*-factor	Mean flux J_V / l min^{-1} m^{-2}	Mean efficiency / %
Nanofiber sponge	NFS-8	This study	–	1.9	41	> 99
Alluvial filter	FILTRODISC™ 2″ BIO SD CH 9P / Celpure® C 1000	Filtrox	Clarifying	137	24	> 99
Depth filter	Seitz® K Series K 900	Pall	Clarifying	7.6	4.4	> 99
Depth filter	FIBRAFIX® AF 31H	Filtrox	Clarifying	8.9	2.3	> 99
Depth filter	Seitz® HS Series HS 2000	Pall	Clarifying	8.5	1.0	> 99
Depth filter	BECOPAD® 450	Eaton	Clarifying	7.1	0.82	> 99
Nanofiber sponge	NFS-26	This study	–	2.2	125	84
Depth filter	PURAFIX® CH 9P	Filtrox	Coarse	11	25	52
Nanofiber mat	NFM-5	This study	–	2.5	1.8	40

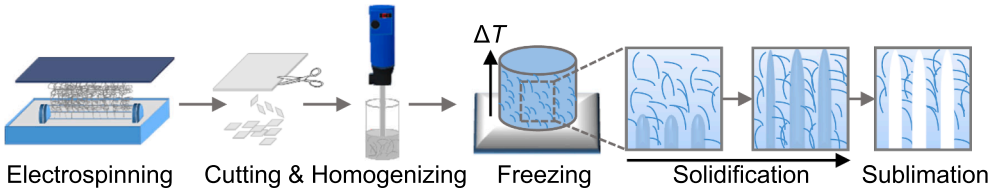

Fig. 1. Preparation of PA6 nanofiber sponge.

500 cycles of 38 % compression. Effective moduli were calculated from the linear regime of stress–strain curves.

The specific surface area (a_{BET}) of the NFS was determined by nitrogen sorption at 77 K with a Quantachrome Autosorb iQ MP (Anton Paar Group AG, Austria) instrument using the multipoint Brunauer-Emmett-Teller (BET) method. The relative pressure range was between 0.12 and 0.3.

3. Results and discussion

3.1. Preparation and characterization of NFM and NFS filters

PA6 NFM were prepared by free surface electrospinning from a (1:2) mixture of formic and acetic acid. An SEM image of NFM-5 with a thickness of 44 ± 7 µm is shown in Fig. 2a. The electrospun nanofibers were free of any defects such as beads or films and had an average diameter of 175 ± 49 nm. This essentially 2D NFM-5 was then processed into highly porous 3D NFS as illustrated in Fig. 2b and Fig. 2c. Both NFS clearly exhibit a hierarchical architecture with large cellular pores and cell walls comprised of PA6 nanofiber fragments which themselves contain smaller pores. Physical parameters of the prepared filter materials are summarized in Table 1. It is important to note that the initial nanofiber building blocks remained intact during processing NFM into NFS. This is observed from the SEM images but also confirmed by determining the specific surface area through N_2 sorption, which remained between a_{BET} = 13 and 15 m^2 g^{-1} throughout the entire process. Such values correspond well with other nanofiber sponges [16,19] and they are close to the geometric specific surface area a_{calc} = 10 m^2 g^{-1} which was derived from the experimental fiber diameter assuming cylindrical nanofibers [29]. The main difference between NFS-26 and NFS-8 was the freezing temperature of the nanofiber suspension, namely –40 °C and –110 °C. The freezing temperature is a simple parameter to change the freezing front velocity of the growing ice crystals which in turn will affect the delicate balance between nanofiber fragments that are pushed away by the growing crystals and those becoming enclosed as previously reported [17,30]. Since the final pore size depends on the crystal size, we were thus able to prepare two types of NFS with identical density but a different pore size of d = 26 ± 14 µm for NFS-26 and d = 8.3 ± 7.3 µm for NFS-8, respectively. The pore size of the 2D NFM-5 was d = 5.3 ± 2.9 µm. The dependence of permeability and filtration efficiency on the pore size of otherwise identical material properties, was demonstrated for aerosol filtration using pullulan/PVA NFS [17,21].

Final stability of the NFS was given by crosslinking the junctions of nanofiber fragments in contact. Several methods have already been reported, such as temperature or UV induced chemical crosslinking

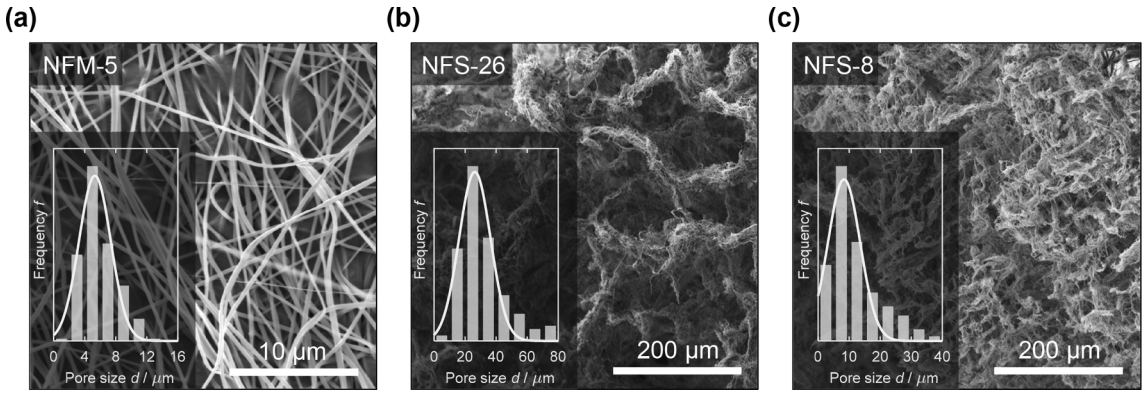

Fig. 2. SEM images and pore size distribution of (a) PA6 based NFM-5 as well as PA6 based NFS frozen at (b) −40, and (c) −110 °C.

[16,17], vapor phase coating [31], or solvent vapor welding [32]. Here, we used a thermal annealing process induced by a thermal phase transition of the PA6 nanofibers close to their melting temperature. The thermographic DSC profiles of PA6 and the NFS before (green body) and after crosslinking are shown in Fig. 3a. The different peaks observed at around 50 °C between the PA6 starting material and the electrospun PA6 fibers in the NFS close to the glass transition temperature of approx. 60 °C are evidencing an ordering process [33]. E.g. release of surface tension generated through the fast fiber drying process during electrospinning [34]. The critical peaks for PA6 annealing are the melting peaks from the different PA6 phases [35,36]. While the pseudohexagonal γ phase is melted at 214 °C (corresponding to the shoulder), the thermodynamically favored monoclinic α phase has a melting point at around 220 °C (main peak). By heating the NFS at 210 °C for crosslinking, the hexagonal fraction of the fibers would melt whereas the monoclinic fraction as the major part of PA6 remained still solid. The melted fraction could act as an adhesive to attach the fibers and render a mechanically stable crosslinked NFS. Compressive strain tests with strain ε of 40 % demonstrated the stability of the NFS structure for 500 loading and unloading cycles, Fig. 3b. No significant decay in stiffness was observed after the 500th loading–unloading cycle with 97 % of the initial maximum stress retained. However, plastic deformation was found from the hysteresis curves with a shape recovery of $>$ 85 % after 500 cycles, Fig. 3b. The effective modulus at 10 % deformation was 5.3 and 3.4 kPa for NFS-26 and NFS-8 respectively, which is in the lower range of NFS based on other polymers, such as pullulan/poly(vinyl alcohol) (PVA) (2.8–21 kPa) [17], polyacrylonitrile (PAN)/SiO_2 (10.6 kPa) [15], poly caprolactone (PCL)/gelatin (10.6–23.4 kPa) [37], poly (vinyl alcohol-co-ethylene) (PVA-co-PE) (11.9 kPa) [38], or chitosan (43 kPa) [19]. The typical stages in the stress–strain curves found in other cellular network with a linear elastic and a Hookean densification regime are not resolved, but a plastic deformation regime [19] is clearly missing.

Stability upon filtration conditions was tested by determining the initial J_0 and final water flux J_∞ for the filtration of 1.5 l deionized water. While the ratio J_∞/J_0 remained constant for NFS-26 and NFS-8 a moderate decline to 0.85 $\pm$ 0.24 was observed for NFM-5, see Table 1. Swelling and partial pore blocking was previously reported for PA6 based membranes [13]. SEM images of NFM-5 before and after water filtration revealed curling of the originally straight fibers which is associated with swelling induced elongation (Supporting Information, Figure S2). The pores of both NFS were too big to reveal any flux dependence with duration of water contact.

While pore size is associated with a sieving effect in filtration, surface interaction through adsorption and inner surface area are determining filtration efficiency as well. The electrokinetic surface potential of the fibers and the yeast cell would reveal important electrostatic interactions. Fig. 3c shows the ζ-potential for yeast cells and the PA6 NFS depending on the pH. The surface of yeast cells was getting negative when the pH of the suspension changed from acidic to basic. However, in basic environment the ζ-potential of the yeast cells was almost constant around –30 mV. Such patterns were also reported in previous studies [39,40]. The ζ-potential of the PA6 NFS dropped linearly from 38 mV to –83 mV when increasing the pH from 2 to 8. Therefore, no attractive electrostatic interaction are expected during the yeast cell filtration experiments performed at pH 5.7.

However, sponge density has an important effect on controlling water flux. It is clear that a denser sponge with more nanofibers, higher amount of micro-pores and thicker pore-walls decreases the water penetration speed through the sponge. The same trend was observed in our previous study on nanoparticle filtration in gas media [21]. It is also proved that the freezing temperature and different sponge pore sizes can also influence the amount of water flux (Table 1).

3.2. Filtration

The dead-end filtration behavior of PA6 nanofiber based filters in terms of filtration efficiency and volumetric flux was studied under hydrostatic conditions with a hydrostatic pressure of 3.5 kPa. Yeast cell suspensions had a mass concentration of $\gamma \approx 1.5$ g l^{-1} dry cell content. The results for the filters NFM-5, NFS-26 and NFS-8 are presented in Fig. 4. The initial volumetric flux for the NFM filter was $J_V = 8.7$ l min^{-1} m^{-2}, whereas the values for the sponge filters NFS-26 and NFS-8 were considerably higher with $J_V = 125$ l min^{-1} m^{-2} and $J_V = 46$ l min^{-1} m^{-2}, respectively. The higher volumetric flux for NFS-26 is given by its larger pores. Commercial depth filters used in germ reducing filtration achieve a similar flux of 98 to 145 l min^{-1} m^{-2}, but such values are obtained at 30-fold pressure (100 kPa instead of 3.5 kPa) [41].

In terms of filtration efficiency, Fig. 4b, the prepared NFM-5 material showed a fast drop of filtration efficiency reaching $\eta \approx 10$ % after 100 ml

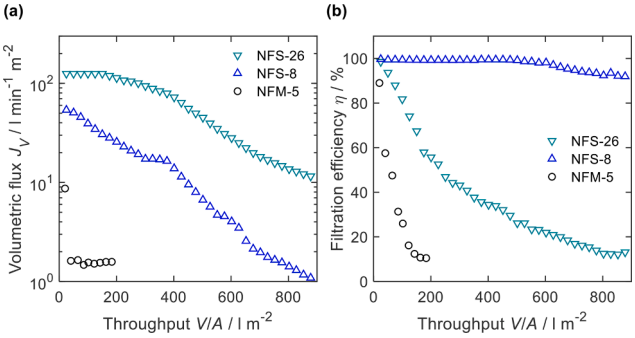

Fig. 4. Yeast cell filtration at 3.5 kPa with NFM-5, NFS-26 and NFS-8; (a) volumetric flux and (b) filtration efficiency.

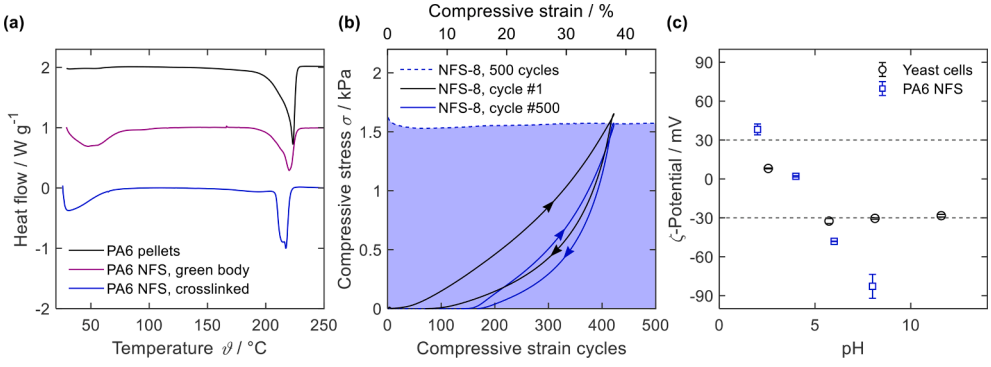

Fig. 3. (a) DSC thermograms (heat rate 10 °C min^{-1}) of PA6 pellets and NFS prepared from electrospun nanofibers before (NFS, green body) and after (NFS, crosslinked) crosslinking; (b) fatigue tests of NFS-8 with ε of 40 % for 500 cycles with maximum stress (bottom axis) and hysteresis curves (top axis); (c) ζ-potential of yeast cells and PA6 NFS depending on pH. Dashed lines indicate the + 30 mV and –30 mV dividing line between stable and unstable suspensions.

filtrate. Thicker NFM filters with smaller pores can achieve a higher filtration efficiency [14], but since the initial volumetric flux was already below the values of the sponge type filters no attempts were made to test thicker materials. The only difference of the sponge type filters was their pore size. The filter with the smaller pores of 8.3 ± 7.3 μm showed a high yeast cell retention of 97.2 ± 2.9 % with decreasing performance after 1000 ml filtrate. NFS-26 with pores of 26 ± 14 μm showed a steady decline in filtration efficiency with an overall cell retention of only 37 ± 24 %. Since yeast cells have a typical size of 8 μm [42], the pores may have been too big to achieve a significant sieving effect. Alternatively, cells may be retained through surface adsorption at the nanofibrous walls of the pores. If this interaction is becoming weaker or if the capacity of the internal pore surface is exhausted, filtration efficiency will drop. Whether sieving or adhesion to the internal surface are dominant can be retrieved from the decline of volumetric flux with filtrate volume, Fig. 4a, assuming different models for the observed filter blocking.

3.3. Filter blocking models

In order to have a clearer understanding on the mechanism of filter blocking, the filtration curves from Fig. 4a were modelled with four different blocking mechanisms reported in the literature: cake filtration, intermediate blocking, standard blocking, complete blocking [43,44]. The governing equations can all be written in a common mathematical form as [45]

$$\frac{d^2\tau}{d\upsilon^2} = k_n \cdot \left(\frac{d\tau}{d\upsilon}\right)^n \quad (1)$$

where υ is the dimensionless volume of filtrate, τ is the dimensionless filtration time, and k_n and n are constants characterizing the blocking model of the filtration process with $n = 0$ for cake filtration, $n = 1$ for intermediate blocking, $n = 3/2$ for standard blocking, and $n = 2$ for complete blocking, Fig. 5. Cake filtration is a frequently observed mechanism, where the accumulation of permeable particles on the upstream side of the filter provides a homogeneous porous layer. After formation of the first cake layer, subsequent filtration occurs on the top of each layer and the filter is only providing the support. Complete blocking, as another possibility, assumes a total clogging of the pore entrance preventing any flow. Intermediate blocking means a mechanism of pore clogging by a fraction of particles with the possibility of some open pores and access to some internal surfaces of the filter. Standard blocking assumes that the pore volume decreases proportionally to the filtrate volume through particles deposited on the pore walls.

Fig. 6a–c show the modelling results for the NFM and NFS filters (details including the root mean square errors (RMSE) are given in the Supporting Information). Based on the fitting results, cake filtration is the dominant blocking mechanism for the filtration of yeast cell suspensions with NFM-5. Fig. 6d shows an SEM image of the upstream surface of the NFM-5 filter illustrating the deposition of a homogeneous layer of cells on the surface of the filter as predicted by the model. Cake formation for nanofiber mats was reported before by different studies [46–48]. For the 3D sponge filters NFS-26 and NFS-8, the dominant blocking mechanism should be standard blocking according to the modelling. The corresponding SEM images of the filter surface, Fig. 6e and f, clearly reveal how the cellular pore structure of the NFS filters prevented cake filtration allowing the cells to penetrate into the pores and to adsorb on their cell walls.

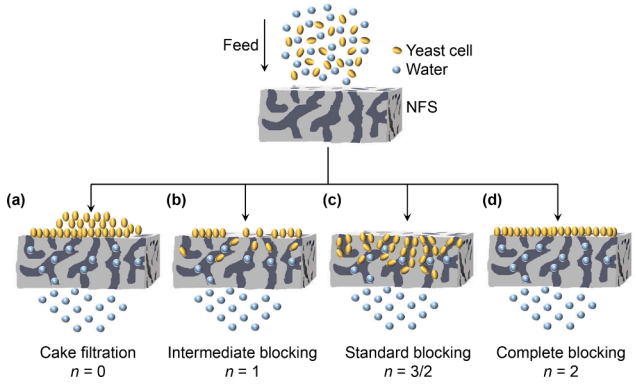

Fig. 5. Models and fitting constants n for filter blocking: (a) cake filtration ($n = 0$), (b) intermediate blocking ($n = 1$), (c) standard blocking ($n = 3/2$), and (d) complete blocking ($n = 2$).

3.4. Commercial depth filter sheets

To rate the dead-end filtration performance of the NFS type filters for yeast cells, several commercially available depth filtration sheets were evaluated under equivalent filtration conditions. The set of commercial filters was selected from several suppliers and covers the relevant range from coarse to clarifying filtration. Filtration efficiency and flux after an equal throughput of 140 l m^{-2} are given in Table 2 (for the decline of flux with throughput see Supporting Information Figure S4). All clarifying filters as well as NFS-8 achieve a filtration efficiency of > 99 %. However, the flux of the commercial filters ($J_V = 0.82$ to 4.4 l min^{-1} m^{-2}) is approx. an order of magnitude lower than for the nanofiber sponge ($J_V = 41$ l min^{-1} m^{-2}). Using the principle of alluvial filtration together with a diatomaceous earth filter aid, a high flux of $J_V = 24$ l min^{-1} m^{-2} was achieved as well. But for the nanofiber sponge, no additional handling of filter aid was necessary. With a coarse depth filter such as PURAFIX® CH 9P, flux was high, but filtration efficiency was only 52 %. Still higher than for the nanofiber mat NFM-5, but the coarse nanofiber sponge NFS-26 showed a higher filtration efficiency of 84 % at fivefold flow.

Even though filtration is known as one of the best industrial methods for removing biomass [1,2], it still requires resources, since filter sheets and filter aids will be disposed after usage. The environmental factor (*E*-factor) is a simple metrics in green chemistry that is defined as the ratio of the mass of resources per mass of product [49]. Here, resources represent the mass of the filter sheet (plus filter aid and housing in case of the disposable alluvial filter) and the product is the dry mass of the filtered biomass. The smaller the *E*-factor, the less resources have been used during the filtration process. Nanofibers with their large specific surface area should allow more surface to solute interactions per unit weight than filters made from larger fibers such as cellulose. This, together with the high porosity and low bulk density is the reason for the small *E*-factors of 1.9 and 2.2 for the NFS filters. Commercial depth filters from cellulose show *E*-factors between 7.1 and 11. The disposable housing of the alluvial filter is mainly responsible for the high *E*-factor of 137 while filter aid and support layer contribute with an *E*-factor of 14.

Here, we studied for the first time the potential of a nanofiber sponge for the filtration of biomass. *Saccharomyces cerevisiae* suspensions were used as a reproducible model system. These results cannot directly be transferred to relevant industrial processes such as beverage filtration [50] or broth from mammalian cells cultures [51] which contain proteins, dissolved and undissolved sugars, other colloidal particles, or ethanol. Regarding pH, the ζ-potential of yeast cells and filter surface, Fig. 3c, suggest, that the sponge filter will adsorb well in the relevant range for beer or wine (pH 3.4 to 4.2) [52]. Using NFS filters with decreased pore size could account for an increased amount of cell debris or a lower flux must be accepted if viscosity is increased due to dissolved sugars.

4. Conclusion

Highly porous 3D nanofiber sponges were prepared from electrospun PA6 nanofibers through a freeze-casting process. Thermal annealing without using chemical crosslinking agents rendered a mechanically

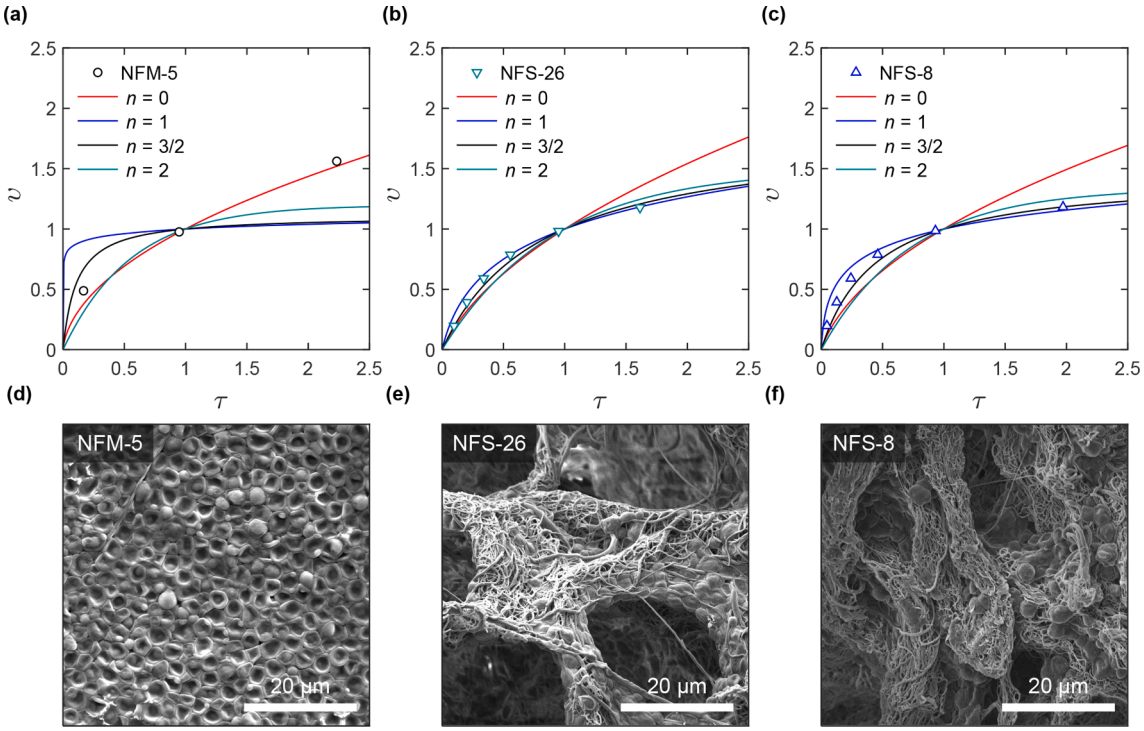

Fig. 6. Fitted blocking models for yeast cell filtration with (a) NFM-5, (b) NFS-26, and (c) NFS-8 and (d–f) corresponding SEM images from the upstream surface of the filters.

stable flexible sponge. The NFS were employed for the filtration of yeast cells from aqueous suspension. As compared to their 2D nanofiber mat counterparts, volumetric flux and filtration efficiency were significantly improved. The pore size of the NFS can easily be tuned during manufacturing through the selected freezing conditions. The filter with the smaller pores showed an initial filtration efficiency of > 99 % while the best volumetric flux was found for the filter with the larger pores. Modelling the blocking mechanisms of the nanofiber mat filter and the nanofiber sponge filter revealed a different filtration mechanism. While cake filtration was dominant for the mat, standard blocking through pore constriction was observed for the NFS filters, meaning that these filter act as true nanofiber based depth filters taking advantage of the surface interactions between the cells and the nanofiber building blocks of the filter.

Nanofiber sponges are a versatile and promising material for filtration applications that have already been used for aerosols, oil/water separation or the removal of dissolved ions. The present work demonstrates their potential as tailored filters for the downstream processing of broth using a PA6 based NFS. Their flow characteristics are superior to state of the art commercial depth filters and less waste is generated during the filtration process thanks to low bulk density and large specific surface area of their nanofiber building blocks. The application of PA6 based NFS is not limited to the present suspension filtration application, but they may also act as a pure adsorbent for the depth filtration of dissolved components, in particular keeping the possibility of PA6 surface functionalization in mind. As for other NFS, PA6 based NFS can also be employed beyond filtration, e.g. in the fields of sound absorption, thermal insulation, and capacitors, or as a material in wound dressing and drug delivery.

CRediT authorship contribution statement

S. Mousavi: Writing – original draft, Invest, igation. **L. Filipová:** Investigation, Validation. **J. Ebert:** Methodology, Conceptualization. **F. J. Heiligtag:** Conceptualization. **R. Daumke:** Conceptualization. **W. Loser:** Conceptualization. **B. Ledergerber:** Methodology. **B. Frank:** Project administration, Formal analysis. **C. Adlhart:** Funding acquisition, Resources, Writing – review & editing.

Declaration of Competing Interest

The authors declare that they have no known competing financial interests or personal relationships that could have appeared to influence the work reported in this paper.

Finances/Acknowledgements

Financial support through Innosuisse grant 25612.1 PFLS and Filtrox AG are kindly acknowledged.

Appendix A. Supplementary material

Supplementary data to this article can be found online at https://doi.org/10.1016/j.seppur.2021.120273.

References

[1] M.A. Chandler, A.L. Zydney, Clarification of yeast cell suspensions by depth filtration, Biotechnol. Prog. 21 (5) (2005) 1552–1557, https://doi.org/10.1021/bp0500821.
[2] P. Linzmeyer, P.K. De Souza, O. Souza, N. Sellin, C. Marangoni, Comparison of different separation methods for solids removal in an ethanol fermentation broth from banana culture waste, Chem. Eng. Trans. 37 (2014) 355–360, https://doi.org/10.3303/CET1437060.
[3] R.H. Bello, O. Souza, N. Sellin, S.H. Medeiros, C. Marangoni, Effect of the microfiltration phase on pervaporation of ethanol produced from banana residues, in: I.A. Karimi, R. Srinivasan (Eds.), Computer Aided Chemical Engineering, Elsevier, 2012, pp. 820–824.
[4] S.G. Redkar, R.H. Davis, Crossflow microfiltration of yeast suspensions in tubular filters, Biotechnol. Prog. 9 (6) (1993) 625–634, https://doi.org/10.1021/bp00024a009.
[5] H.P. Hsieh, Inorganic membranes for separation and reaction, Elsevier Science B.V, Amsterdam, 1996.
[6] A.L. Zydney, R. van Reis, in: Comprehensive Biotechnology, Elsevier, 2011, pp. 499–520, https://doi.org/10.1016/B978-0-08-088504-9.00440-2.
[7] S. Kang, A. Subramani, E. Hoek, M. Deshusses, M. Matsumoto, Direct observation of biofouling in cross-flow microfiltration: Mechanisms of deposition and release,

J. Membr. Sci. 244 (1-2) (2004) 151–165, https://doi.org/10.1016/j.memsci.2004.07.011.
[8] V.M. da Matta, R. de Andrade Medronho, A new method for yeast recovery in batch ethanol fermentations: Filter aid filtration followed by separation of yeast from filter aid using hydrocyclones, Bioseparation 9 (2000) 43–53, https://doi.org/10.1023/A:1008145419175.
[9] M. Mota, J.A. Teixeira, A. Yelshin, Baker's yeast filtration through mixed beds of filtration aids and large glass beads. in: 9th International Chemical Engineering Conference, Departamento de Engenharia Química da Universidade de Coimbra, 2005.
[10] M. Chandler, A. Zydney, Effects of membrane pore geometry on fouling behavior during yeast cell microfiltration, J. Membr. Sci. 285 (1-2) (2006) 334–342, https://doi.org/10.1016/j.memsci.2006.09.002.
[11] S. Kuiper, C.J.M. van Rijn, W. Nijdam, M.C. Elwenspoek, Development and applications of very high flux microfiltration membranes, J. Membr. Sci. 150 (1) (1998) 1–8, https://doi.org/10.1016/S0376-7388(98)00197-5.
[12] A.J. Bromley, R.G. Holdich, I.W. Cumming, Particulate fouling of surface microfilters with slotted and circular pore geometry, J. Membr. Sci. 196 (1) (2002) 27–37, https://doi.org/10.1016/S0376-7388(01)00573-7.
[13] A.M.D. Leite, E.M. Araujo, V. Medeiros, R.A. da Paz, H.d.L. Lira, Comparative study of membranes obtained from PA6 and PA66/national clay nanocomposites, in: A. Hashim (Ed.), Advances in Nanocomposite Technology, InTech, Croatia, 2011, pp. 115–131.
[14] S.M. Lemma, A. Esposito, M. Mason, L. Brusetti, S. Cesco, M. Scampicchio, Removal of bacteria and yeast in water and beer by nylon nanofibrous membranes, J. Food Eng. 157 (2015) 1–6, https://doi.org/10.1016/j.jfoodeng.2015.02.005.
[15] Y. Si, J. Yu, X. Tang, J. Ge, B. Ding, Ultralight nanofibre-assembled cellular aerogels with superelasticity and multifunctionality, Nat. Commun. 5 (2014) 5802, https://doi.org/10.1038/ncomms6802.
[16] G. Duan, S. Jiang, V. Jérôme, J.H. Wendorff, A. Fathi, J. Uhm, V. Altstädt, M. Herling, J. Breu, R. Freitag, S. Agarwal, A. Greiner, Ultralight, soft polymer sponges by self-assembly of short electrospun fibers in colloidal dispersions, Adv. Funct. Mater. 25 (19) (2015) 2850–2856, https://doi.org/10.1002/adfm.201500001.
[17] F. Deuber, S. Mousavi, M. Hofer, C. Adlhart, Tailoring pore structure of ultralight electrospun sponges by solid templating, ChemistrySelect 1 (18) (2016) 5595–5598, https://doi.org/10.1002/slct.201601084.
[18] M. Merk, O. Chirikian, C. Adlhart, 3D PCL/gelatin/genipin nanofiber sponge as scaffold for regenerative medicine, Materials 14 (2021) 2006, https://doi.org/10.3390/ma14082006.
[19] P. Risch, C. Adlhart, A chitosan nanofiber sponge for oyster-inspired filtration of microplastics, ACS Appl. Polymer Mater. 3 (9) (2021) 4685–4694, https://doi.org/10.1021/acsapm.1c00799.
[20] M. Dilamian, M. Joghataei, Z. Ashrafi, C. Bohr, S. Mathur, H. Maleki, From 1D electrospun nanofibers to advanced multifunctional fibrous 3D aerogels, Appl. Mater. Today 22 (2021) 100964, https://doi.org/10.1016/j.apmt.2021.100964.
[21] F. Deuber, S. Mousavi, L. Federer, M. Hofer, C. Adlhart, Exploration of ultralight nanofiber aerogels as particle filters: Capacity and efficiency, ACS Appl. Mater. Interfaces 10 (10) (2018) 9069–9076, https://doi.org/10.1021/acsami.8b00455.
[22] F. Deuber, S. Mousavi, L. Federer, C. Adlhart, Amphiphilic nanofiber-based aerogels for selective liquid absorption from electrospun biopolymers, Adv. Mater. Interfaces 4 (12) (2017) 1700065, https://doi.org/10.1002/admi.201700065.
[23] Y. Si, Q. Fu, X. Wang, J. Zhu, J. Yu, G. Sun, B. Ding, Superelastic and superhydrophobic nanofiber-assembled cellular aerogels for effective separation of oil/water emulsions, ACS Nano 9 (4) (2015) 3791–3799, https://doi.org/10.1021/nn506633b.
[24] T. Pirzada, Z. Ashrafi, W. Xie, S.A. Khan, Cellulose silica hybrid nanofiber aerogels: From sol-gel electrospun nanofibers to multifunctional aerogels, Adv. Funct. Mater. 30 (5) (2020) 1907359, https://doi.org/10.1002/adfm.201907359.
[25] X. Hou, R. Zhang, D. Fang, Flexible, fatigue resistant, and heat-insulated nanofiber-assembled polyimide aerogels with multifunctionality, Polym. Test. 81 (2020) 106246, https://doi.org/10.1016/j.polymertesting.2019.106246.
[26] S. Mousavi, F. Deuber, S. Petrozzi, L. Federer, M. Aliabadi, F. Shahraki, C. Adlhart, Efficient dye adsorption by highly porous nanofiber aerogels, Colloids Surf., A 547 (2018) 117–125, https://doi.org/10.1016/j.colsurfa.2018.03.052.
[27] V. Guarino, A. Guaccio, P.A. Netti, L. Ambrosio, Image processing and fractal box counting: user-assisted method for multi-scale porous scaffold characterization, J. Mater. Sci. - Mater. Med. 21 (12) (2010) 3109–3118, https://doi.org/10.1007/s10856-010-4163-9.
[28] L. Safinia, A. Mantalaris, A. Bismarck, Nondestructive technique for the characterization of the pore size distribution of soft porous constructs for tissue engineering, Langmuir 22 (7) (2006) 3235–3242, https://doi.org/10.1021/la051762g.
[29] S. Mousavi, F. Shahraki, M. Aliabadi, A. Haji, F. Deuber, C. Adlhart, Surface enriched nanofiber mats for efficient adsorption of Cr(VI) inspired by nature, J. Environ. Chem. Eng. 7 (1) (2019) 102817, https://doi.org/10.1016/j.jece:2018.102817.
[30] F. Deuber, C. Adlhart, From Short Electrospun nanofibers to ultralight aerogels with tunable pore structure, CHIMIA Int. J. Chem. 71 (4) (2017) 236–240, https://doi.org/10.2533/chimia.2017.236.
[31] G. Duan, S. Jiang, T. Moss, S. Agarwal, A. Greiner, Ultralight open cell polymer sponges with advanced properties by PPX CVD coating, Polym. Chem. 7 (15) (2016) 2759–2764, https://doi.org/10.1039/C6PY00339G.
[32] Y. Shen, D. Li, B. Deng, Q. Liu, H. Liu, T. Wu, Robust polyimide nano/microfibre aerogels welded by solvent-vapour for environmental applications, R. Soc. Open Sci. 6 (8) (2019) 190596, https://doi.org/10.1098/rsos.190596.
[33] J.-R. Xu, X.-K. Ren, T. Yang, X.-Q. Jiang, W.-Y. Chang, S. Yang, A. Stroeks, E.-Q. Chen, Revisiting the thermal transition of β-form polyamide-6: Evolution of structure and morphology in uniaxially stretched films, Macromolecules 51 (1) (2018) 137–150, https://doi.org/10.1021/acs.macromol.7b01827.
[34] R. Nirmala, R. Navamathavan, M.H. El-Newehy, H.Y. Kim, Preparation and characterization of electrospun ultrafine polyamide-6 nanofibers, Polym. Int. 60 (10) (2011) 1475–1480, https://doi.org/10.1002/pi.3105.
[35] C.W. Bunn, E. Garner, W.L. Bragg, The crystal structures of two polyamides ('nylons') proceedings of the royal society of london. Series A. Mathematical Phys. Sci. 189 (1947) 39–68, https://doi.org/10.1098/rspa.1947.0028.
[36] Y.i. Liu, L.i. Cui, F. Guan, Y.i. Gao, N.E. Hedin, L. Zhu, H. Fong, Crystalline morphology and polymorphic phase transitions in electrospun nylon-6 nanofibers, Macromolecules 40 (17) (2007) 6283–6290, https://doi.org/10.1021/ma070039p.
[37] M. Merk, O. Chirikian, C. Adlhart, 3D PCL/gelatin/genipin nanofiber sponge as scaffold for regenerative medicine, Materials 14 (8) (2021) 2006, https://doi.org/10.3390/ma14082006.
[38] Q. Liu, J. Chen, T. Mei, X. He, W. Zhong, K.e. Liu, W. Wang, Y. Wang, M. Li, D. Wang, A facile route to the production of polymeric nanofibrous aerogels for environmentally sustainable applications, J. Mater. Chem. A 6 (8) (2018) 3692–3704, https://doi.org/10.1039/C7TA10107D.
[39] S. Tazhibaeva, K. Musabekov, A. Orazymbetova, A. Zhubanova, Surface properties of yeast cells, Colloid J. 65 (2003) 122–124, https://doi.org/10.1023/A:1022391613491.
[40] K. Tálos, T. Pernyeszi, C. Majdik, A. Hegedűsova, C. Páger, Cadmium biosorption by baker's yeast in aqueous suspensions, J. Serb. Chem. Soc. 77 (4) (2012) 549–561, https://doi.org/10.2298/JSC110520181T.
[41] Technical Data Sheet, Filtrox (2018).
[42] M. Zakhartsev, M. Reuss, Cell size and morphological properties of yeast Saccharomyces cerevisiae in relation to growth temperature, FEMS Yeast Res. 18 (2018), https://doi.org/10.1093/femsyr/foy052.
[43] J. Hermia, Constant pressure blocking filtration laws: Application to power-law non-Newtonian fluids, Transactions of the Institution of Chemical Engineers 60 (1982) 183–187.
[44] M. Shirato, T. Aragaki, E. Iritani, Blocking filtration laws for filtration of power-law non-Newtonian fluids, J. Chem. Eng. Jpn. 12 (1979) 162–164.
[45] K. Konieczny, J. Rafa, Modeling of the membrane filtration process of natural waters, Polish J. Envir. Studies 9 (2000) 57–64, https://doi.org/10.1016/S0011-9164(02)00234-5.
[46] C.-C. Ho, A.L. Zydney, A combined pore blockage and cake filtration model for protein fouling during microfiltration, J. Colloid Interface Sci. 232 (2) (2000) 389–399, https://doi.org/10.1006/jcis.2000.7231.
[47] M.C.V. Vela, S.Á. Blanco, J.L. García, E.B. Rodríguez, Analysis of membrane pore blocking models applied to the ultrafiltration of PEG, Sep. Purif. Technol. 62 (3) (2008) 489–498, https://doi.org/10.1016/j.seppur.2008.02.028.
[48] Y.i. Zheng, W. Zhang, B. Tang, J. Ding, Y.i. Zheng, Z. Zhang, Membrane fouling mechanism of biofilm-membrane bioreactor (BF-MBR): Pore blocking model and membrane cleaning, Bioresour. Technol. 250 (2018) 398–405, https://doi.org/10.1016/j.biortech.2017.11.036.
[49] R.A. Sheldon, The E Factor: Fifteen years on, Green Chem. 9 (2007) 1273–1283, https://doi.org/10.1039/b713736m.
[50] A. Onur, A. Ng, G. Garnier, W. Batchelor, Engineering cellulose fibre inorganic composites for depth filtration and adsorption, Sep. Purif. Technol. 203 (2018) 209–216, https://doi.org/10.1016/j.seppur.2018.04.038.
[51] N. Singh, K. Pizzelli, J.K. Romero, J. Chrostowski, G. Evangelist, J. Hamzik, N. Soice, K.S. Cheng, Clarification of recombinant proteins from high cell density mammalian cell culture systems using new improved depth filters, Biotechnol. Bioeng. 110 (7) (2013) 1964–1972, https://doi.org/10.1002/bit.24848.
[52] S.H. Jeon, N.H. Kim, M.B. Shim, Y.W. Jeon, J.H. Ahn, S.H. Lee, I.G. Hwang, M. S. Rhee, Microbiological diversity and prevalence of spoilage and pathogenic bacteria in commercial fermented alcoholic beverages (Beer, Fruit Wine, Refined Rice Wine, and Yakju), J. Food Prot. 78 (2015) 812–818, https://doi.org/10.4315/0362-028X.JFP-14-431.